Chinese Physics Letters

LETTER

Spin Quadrupolar Order in d-wave Unconventional Magnetism

Cite as: Jian-Keng Yuan *et al*. 2026 *Chin. Phys. Lett.* **43** 090703

DOI CSTR

Recommended Articles

Unconventional Compensated Magnetic Material $LaMn_2SbO_6$

Xiao-Yao Hou, Ze-Feng Gao, Huan-Cheng Yang, Peng-Jie Guo, and Zhong-Yi Lu
Chin. Phys. Lett. **42**, 070712 (2025)

Helicity-Controlled Spin Hall Angle in 2D Altermagnets with Rashba Spin-Orbit Coupling

Weiwei Chen, Longhai Zeng, and W. Zhu
Chin. Phys. Lett. **42**, 017201 (2025)

Magnon Splitting and Magnon Spin Transport in Altermagnets

Kun Wu, Jianting Dong, Meng Zhu, Fanxing Zheng, and Jia Zhang
Chin. Phys. Lett. **42**, 070702 (2025)

Tunneling Magnetoresistance Effect in Altermagnetic Tunnel Junctions with g-Wave Splitting

Xinlu Li, Meng Zhu, Jianting Dong, Kun Wu, Fanxing Zheng, and Jia Zhang
Chin. Phys. Lett. **42**, 100701 (2025)

A series journal of Chinese Physical Society distributed by IOP Publishing

Chinese Physics Letters

Chin. Phys. Lett. **43** 090703 (2026)

LETTER

DOI: 10.1088/0256-307X/43/9/090703
CSTR: 32039.14.0256-307X.43.9.090703

Spin Quadrupolar Order in d-wave Unconventional Magnetism

Jian-Keng Yuan[1,2], Zhiming Pan[3,*], and Congjun Wu[2,4,5,6,*]

[1]Department of Physics, Fudan University, Shanghai 200433, China
[2]New Cornerstone Science Laboratory, Department of Physics, School of Science, Westlake University, Hangzhou 310024, China
[3]Department of Physics, Xiamen University, Xiamen 361005, China
[4]Institute for Theoretical Sciences, Westlake University, Hangzhou 310024, China
[5]Key Laboratory for Quantum Materials of Zhejiang Province, School of Science, Westlake University, Hangzhou 310024, China
[6]Institute of Natural Sciences, Westlake Institute for Advanced Study, Hangzhou 310024, China

*Corresponding authors. Email: panzhiming@xmu.edu.cn; wucongjun@westlake.edu.cn

Unconventional magnetism represents a class of metallic states whose Fermi surfaces exhibit spin-dependent splittings under the nontrivial representations of the rotation group. The d-wave α-phase of unconventional magnetism provides a continuum realization of the nonrelativistic spin-splitting physics described in crystals within the framework of altermagnetism; the two share the same symmetry under rotation. In this work, we investigate how the associated momentum-space spin quadrupole manifests itself in the real-space spin structure of a crystal. Within linear-response theory, we calculate the spin-charge cross-susceptibility of the d-wave state in a weak nonmagnetic periodic scalar potential. The combined symmetry of the d-wave α-phase requires the response to change sign between two symmetry-related reciprocal-lattice vectors, producing an intra-unit-cell d-wave spin-density modulation without enlarging the unit cell. The resulting real-space spin modulation is induced by the scalar lattice potential rather than being a consequence of spontaneous symmetry breaking. It thus provides a real-space linear-response signature of the even-parity momentum-space spin multipole.

Introduction

Itinerant ferromagnetism exhibits a uniform spin polarization over the Fermi surface, whose symmetry is analogous to conventional s-wave superconductivity. Similarly, drawing inspiration from higher partial-wave pairing in superconductivity, the concept of magnetic ordering can also be extended to the spin channel when spin-orbit coupling (SOC) is negligible [1,2]. This phenomenon, termed "unconventional magnetism" (UM) [3,4], forms nontrivial representations of the rotational group. This phase exhibits an intrinsic, anisotropic distortion of the Fermi surface, establishing a spin-splitting effect independent of relativistic SOC. A prominent example is the collinear α-phase in the d-wave channel, which breaks time-reversal symmetry but preserves inversion symmetry [2,5,6].

Recently, UM, especially the α-phase in even partial-wave channels, has attracted great attention under the name of "altermagnetism" [7–9]. In altermagnets, the real-space periodicity of the magnetic structure is the same as that of the underlying crystal lattice. Such states exhibit spin-group symmetry, i.e., a combination of different types of orbital and spin rotations. This symmetry classification, reliant on the framework of spin space groups [10–14], organizes these magnetic orders and dictates their transport properties. A common example of spin group symmetry is a spatial rotation about the z-axis by an angle of $\pi/2$, followed by a π-rotation in spin space. Unlike conventional antiferromagnets, this spin structure results in spin-split Fermi surfaces in the absence of macroscopic net magnetization or SOC [15–23]. The interplay between the electron band structure and lattice-compatible magnetic orders gives rise to rich physical phenomena [24–29], leading to novel spintronic applications [30–36], anomalous Hall effects [37–47], and topological phenomena [48–56].

The d-wave α-phase of UM is commonly regarded as a precursor continuum study of the same nonrelativistic spin-splitting physics in crystals termed as altermagnetism. In the d-wave α-phase, the spin-quadrupolar order manifests itself as a momentum-space d-wave distortion without breaking translation symmetry [2,4]. By contrast, the crystalline altermagnets start with the intra-unit-cell magnetic structure exhibiting the d-wave pattern [7,8]. It induces the d-wave spin splitting over Fermi surfaces when the system is metallic. In contrast, a natural question arises: If a lattice potential is imposed on the d-wave α-phase of UM, will a spin structure be generated in real space, and if so, what is the symmetry pattern?

In this work, we study how the momentum-space spin quadrupole of the d-wave α phase manifests itself in the spin-density response to a weak nonmagnetic periodic scalar potential. Within linear-response theory, we calculate the static spin-charge cross-susceptibility and determine the induced real-space spin distribution. The combined symmetry of the d-wave state enforces opposite signs of the susceptibility at a pair of symmetry-related reciprocal-lattice vectors, producing an intra-unit-cell d-wave spin-density modulation without enlarging the unit cell. In the low-density limit, the cross-susceptibility is proportional to the spin-quadrupole order in momentum space. The resulting real-space staggered spin modulation is therefore a linear-response manifestation of the preexisting momentum-space d-wave UM order.

d-Wave Magnetism in Crystals

In 2D, the symmetry-allowed low-energy effective Hamiltonian for a d-wave α-phase UM could be described by the following continuum model [2],

$$H_0 = -\frac{1}{2m}[\nabla^2 + Q(\partial_x^2 - \partial_y^2)\sigma_z] - \mu, \tag{1}$$

where the Pauli matrix σ_z acts in spin space, m is the effective mass, and μ is the chemical potential. Here, we have set $\hbar = 1$ for simplicity. The first term represents the isotropic kinetic energy, while the second term captures the d-wave UM order.

In momentum space, the low-energy effective spectrum of the

Received 13 May 2026; accepted 15 August 2026; published 8 September 2026
© 2026 Chinese Physical Society and IOP Publishing Ltd. All rights, including for text and data mining, AI training, and similar technologies, are reserved.

Check for updates

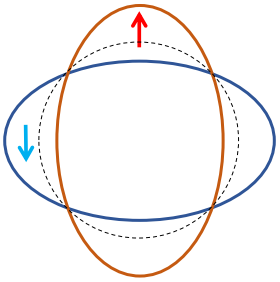

Fig. 1. The Fermi surfaces of d-wave α-phase unconventional magnetic states. The distorted Fermi surfaces are obtained from the Hamiltonian in Eq. (1) and reflects the specific symmetry of d-wave magnetic states in Eq. (7).

d-wave α-phase in Eq. (1) is given by

$$\xi_\sigma(\boldsymbol{k}) = \frac{1}{2m}[\boldsymbol{k}^2 + Q(k_x^2 - k_y^2)\sigma - k_\mathrm{f}^2], \tag{2}$$

where $\sigma = \pm 1$ denotes the spin-up and spin-down projections, respectively, and k_f is the effective Fermi momentum characterizing the unperturbed chemical potential $\mu = k_\mathrm{f}^2/2m$. Crucially, this energy spectrum dictates a specific symmetry under a $\pi/2$ rotation around the z-axis, as shown in Fig. 1. This order breaks both time-reversal $\mathcal{T}$ and C_4 rotational symmetries but preserves the combined $C_4\mathcal{T}$ symmetry, resulting in a spin-dependent anisotropic effective mass. The dimensionless parameter Q characterizes the strength of the d-wave magnetic order. We restrict Q to the range $-1 < Q < 1$ so that the kinetic energy remains positive definite in all directions and the continuum model is stable around the Γ point.

While Eq. (1) captures the spin-splitting of altermagnetism in a continuum, it does not incorporate the Brillouin-zone periodicity of a crystal. To investigate the interplay between the d-wave spin-splitting and lattice translation symmetry, we adopt a nearly-free-electron (empty-lattice) approach. For simplicity, we subject this continuum model to a weak periodic crystal potential of a 2D square lattice, expressed in real space as

$$V(x,y) = V_0(\cos Gx + \cos Gy), \tag{3}$$

where V_0 is the potential strength and G is the magnitude of the primitive reciprocal lattice vector. Upon Fourier transformation, the periodic potential generates scattering processes involving reciprocal lattice vectors:

$$V(\boldsymbol{q}) = \frac{V_0}{2} \sum_{\boldsymbol{G}\in\{\pm\boldsymbol{G}_1,\pm\boldsymbol{G}_2\}} \delta_{\boldsymbol{q},\boldsymbol{G}} \tag{4}$$

where $\boldsymbol{G}_1 = (G,0)$ and $\boldsymbol{G}_2 = (0,G)$. This phenomenological framework allows us to qualitatively capture the generic Fermi surface properties of d-wave magnetic states in a crystal without resorting to a complex tight-binding model.

Spin Response

Although spin-density waves can arise from Fermi surface nesting or strong correlations, a spin-density modulation can also be induced in a d-wave α-phase. Due to the intrinsic distortion of the spin-split Fermi surfaces, a purely nonmagnetic scalar potential can directly induce a static spin density modulation. Here, we use the linear-response theory to calculate this spin-charge cross-response induced by a weak periodic crystal potential; see the Appendix for the details.

To determine the induced real-space spin distribution, we evaluate the static spin-charge cross-susceptibility. The bare Green's function is diagonal in spin space:

$$G(\boldsymbol{k}, \mathrm{i}\omega_n) = \frac{1}{2}\left(\frac{1+\sigma_z}{\mathrm{i}\omega_n - \xi_+(\boldsymbol{k})} + \frac{1-\sigma_z}{\mathrm{i}\omega_n - \xi_-(\boldsymbol{k})}\right), \tag{5}$$

where ω_n represents fermionic Matsubara frequency. The correlation function χ between the z-component of the spin density and the

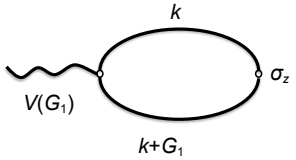

Fig. 2. Bubble diagram for the static spin-charge cross-susceptibility $\chi(\boldsymbol{G}_1)$.

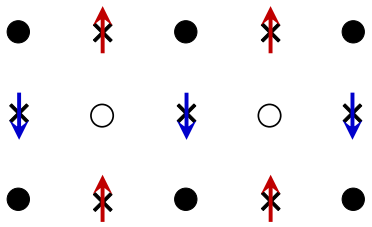

Fig. 3. The crystal potential (black) and spin response (arrows) in d-wave unconventional magnetic states. Black solid circles, open circles, and crosses represent the maxima, minima, and saddle points of the crystal potential, respectively. Red and blue arrows denote the positive and negative extrema of the induced spin response.

charge density at a reciprocal lattice vector $\boldsymbol{G}_1$ is given by (see Fig. 2),

$$\begin{aligned}\chi(\boldsymbol{G}_1) &= T\sum_{\mathrm{i}\omega_n}\int_{\mathrm{BZ}}\frac{\mathrm{d}^2\boldsymbol{k}}{(2\pi)^2}\mathrm{tr}[G(\boldsymbol{k},\mathrm{i}\omega_n)G(\boldsymbol{k}+\boldsymbol{G}_1,\mathrm{i}\omega_n)\sigma_z] \\ &= \int_{\mathrm{BZ}}\frac{\mathrm{d}^2\boldsymbol{k}}{(2\pi)^2}\sum_{\sigma=\pm1}\sigma\frac{n_\mathrm{F}[\xi_\sigma(\boldsymbol{k})] - n_\mathrm{F}[\xi_\sigma(\boldsymbol{k}+\boldsymbol{G}_1)]}{\xi_\sigma(\boldsymbol{k}) - \xi_\sigma(\boldsymbol{k}+\boldsymbol{G}_1)},\end{aligned} \tag{6}$$

where BZ denotes the first Brillouin zone and $n_\mathrm{F}(\epsilon)$ is the Fermi-Dirac distribution. We define the rotation operator R by $R(k_x,k_y) = (-k_y,k_x)$. The spectrum then satisfies:

$$\xi_\sigma(R\boldsymbol{k}) = \xi_{-\sigma}(\boldsymbol{k}). \tag{7}$$

Under this rotation, $\boldsymbol{k} \to R\boldsymbol{k}$, the Brillouin zone of the square lattice remains invariant. By utilizing the spectral symmetry in Eq. (7) and transforming the integration variables, one can rigorously show that the cross-susceptibility is antisymmetric under the C_4 rotation:

$$\chi(R\boldsymbol{G}_1) = -\chi(\boldsymbol{G}_1). \tag{8}$$

Since $\boldsymbol{G}_2 = R\boldsymbol{G}_1$ and inversion symmetry gives $\chi(\boldsymbol{G}) = \chi(-\boldsymbol{G})$, the susceptibilities satisfy the relation:

$$\chi(\pm\boldsymbol{G}_1) = -\chi(\pm\boldsymbol{G}_2) = \chi. \tag{9}$$

By summing over the Fourier components of the crystal potential in Eq. (3), we obtain the induced real-space spin density up to first order in V_0:

$$S_z(\boldsymbol{r}) = \chi V_0(\cos Gx - \cos Gy). \tag{10}$$

This arises from the combined effects of the crystal potential and the d-wave UM order. Comparing the spatial profile of the periodic potential $V(\boldsymbol{r})$ with the induced spin density $S_z(\boldsymbol{r})$, we observe that the positive and negative extrema of the spin response occur at the saddle points of the underlying periodic potential (i.e., where $V(\boldsymbol{r}) = 0$), as shown in Fig. 3.

In the paramagnetic normal state (where $Q = 0$), the cross-susceptibility χ vanishes, and consequently, no spin response is induced. To quantitatively elucidate the precise role of the d-wave UM order in driving this spin response, we evaluate the susceptibility χ as a function of the order parameter Q.

To make the discussion concrete, we focus on the low-electron-density regime at zero temperature. In this limit, the Fermi momentum is small, and the Fermi surfaces remain tightly confined around the Γ point, far from the boundaries of the Brillouin zone. The relevant electron momenta satisfy $|\boldsymbol{k}| \ll G/2$. By expanding the energy denominator to the leading order in $|\boldsymbol{k}|/G$, we obtain:

$$\frac{1}{\xi_\sigma(\boldsymbol{k})-\xi_\sigma(\boldsymbol{k}+\boldsymbol{G}_1)}=-\frac{2m}{G^2(1+\sigma Q)}. \tag{11}$$

At zero temperature, the Fermi-Dirac distribution reduces to a step function, $n_{\mathrm{F}}(\epsilon)=\Theta(-\epsilon)$, where $\Theta(\epsilon)=0$ for $\epsilon\le 0$ and $\Theta(\epsilon)=1$ for $\epsilon>0$. Equation (6) then yields

$$\chi=-\frac{mk_{\mathrm{f}}^2}{\pi G^2}\frac{1}{\sqrt{1-Q^2}}\left(\frac{1}{1+Q}-\frac{1}{1-Q}\right). \tag{12}$$

The analytical expression captures the underlying physics. As expected, the d-wave UM order distorts the initially isotropic Fermi surface into spin-dependent ellipses. This d-wave anisotropy yields a nonvanishing cross-susceptibility, converting the purely scalar crystal potential into the staggered spin density modulation described in Eq. (10). The susceptibility χ in Eq. (12) is proportional to Q for weak ordering and grows monotonically as the order parameter increases. The emergence of the d-wave magnetic phase ($Q\neq 0$) acts as the driver for generating this spatially modulated spin response. Moreover, the cross-susceptibility formally diverges as $|Q|\to 1$ within this approximation.

Quadrupole and Susceptibility

To elucidate the physical origin of the induced spin response, it will be instructive to connect the macroscopic cross-susceptibility to the intrinsic geometric properties of the unperturbed altermagnetic ground state. We achieve this by examining the momentum-space spin quadrupole moment, which characterizes the d-wave spin-splitting. It is defined as:

$$Q_{k_\mu k_\nu}=\int_{\mathrm{BZ}}\frac{\mathrm{d}^2\boldsymbol{k}}{(2\pi)^2}\sum_{\sigma=\pm1}\sigma n_{\mathrm{F}}[\xi_\sigma(\boldsymbol{k})]k_\mu k_\nu, \tag{13}$$

where $\mu,\nu=x,y$ in 2D. Owing to the mirror symmetries, the off-diagonal quadrupole component vanishes, i.e., $Q_{k_xk_y}=0$. Furthermore, under a $\pi/2$ spatial rotation $\boldsymbol{k}\to R\boldsymbol{k}$, the integration domain remains invariant. By utilizing the spectral symmetry dictated by the altermagnetic order, $\xi_\sigma(R\boldsymbol{k})=\xi_{-\sigma}(\boldsymbol{k})$ in Eq. (7), and performing a change of integration variables, one can show that the diagonal components satisfy:

$$Q_{k_y^2}=-Q_{k_x^2}. \tag{14}$$

This antisymmetric relation is the microscopic origin of the d-wave macroscopic response, mirroring the discrete symmetry of the spin-charge susceptibility in Eqs. (8) and (9).

To quantitatively establish the relationship between the linear response susceptibility and this intrinsic ground-state property, we evaluate $Q_{k_x^2}$ at zero temperature. Integrating over the spin-split elliptical Fermi seas yields the analytical result:

$$Q_{k_x^2}=\frac{k_{\mathrm{f}}^4}{16\pi\sqrt{1-Q^2}}\left(\frac{1}{1+Q}-\frac{1}{1-Q}\right). \tag{15}$$

Comparing this intrinsic quadrupole moment with the expression for the cross-susceptibility derived in Eq. (12), we uncover an algebraic relation:

$$\chi=-\frac{16m}{G^2k_{\mathrm{f}}^2}Q_{k_x^2}. \tag{16}$$

The induced spin-charge cross-susceptibility is proportional to the intrinsic spin quadrupole moment in momentum space. Both quantities vanish in the normal phase ($Q=0$), and their magnitudes increase with $|Q|$ within the present model. From a physical standpoint, while $Q_{k_x^2}$ serves as a microscopic order parameter that breaks time-reversal and rotational symmetries, the cross-susceptibility χ acts as a macroscopic response coefficient associated with this order. Measuring this anisotropic spin response to a scalar charge potential offers a signature of the hidden d-wave spin-splitting.

Discussion

The induced intra-unit-cell spin-density modulation is a linear-response manifestation of the underlying momentum-space d-wave UM order, rather than a separate spontaneous magnetic order. Its d-wave transformation property is fixed by symmetry, whereas its magnitude and precise relation to the momentum-space spin quadrupole $Q_{k_x^2}$ depend on the microscopic realization.

In the above analysis, we have used the empty-lattice approximation in analytic studies for clarity. Despite this, our central result, i.e., the emergence of the staggered spin-density modulation without enlarging unit cells, is robust as protected by symmetry. The d-wave symmetry of the spin-charge cross-susceptibility, $\chi(R\boldsymbol{G}_1)=-\chi(\boldsymbol{G}_1)$, is based on the combined $C_4\mathcal{T}$ symmetry. In realistic materials with strong crystal potential or larger electron densities, band reconstructions near Brillouin zone boundaries occur. These effects would only quantitatively renormalize the spin-density responses studies above without modifying its qualitative features. Detailed investigations are beyond the scope of this work and will be deferred to a later publication.

Experimentally, recent scanning tunneling microscopy measurements have imaged defect-induced electronic patterns reflecting the characteristic rotational anisotropy of d-wave altermagnetism [57]. Although these measurements do not directly probe the periodic spin-density modulation considered here, they demonstrate that local scattering can reveal the underlying spin-charge anisotropy. A standard $\boldsymbol{T}$-matrix treatment incorporating a realistic band structure can be used to model the corresponding impurity response. Spin-polarized scanning tunneling microscopy could further probe the predicted sign reversal between the rotation-related Fourier components along the a and b directions.

In real altermagnetic materials, finite SOC breaks the independent spin-group symmetry assumed above, and spin is no longer a good quantum number. Since SOC is time-reversal even, it cannot by itself generate a static spin-density response to the scalar potential considered here. Nevertheless, SOC breaks inversion symmetry, which could generate the Dzyaloshinskii–Moriya (DM) interaction for the real-space spin distributions. In the case of weak SOC, the DM interaction would not fundamentally destroy staggered spin-density modulation polarized along the z-axis but could induce spin canting with small transverse components.

Our mechanism works for UM orders with even parity, in which time-reversal symmetry is broken, such that real-space spin structures are allowed. In contrast, for UM orders with odd parity, time-reversal symmetry is preserved, which suppresses real space magnetic structures. For the p-wave case, the real space structure induced by the scalar lattice potential is of the bond-centered spin-current type. For example, on a lattice bond of $\langle ij\rangle$, the real space order can be represented by D_{ij}^{μ}, where μ refers to the direction in spin space; hence, it is a DM-vector type order. This is an interesting topic for future investigations.

Conclusion

In summary, we have theoretically investigated the spin-charge cross-response in a 2D d-wave UM (altermagnetic) state subjected to a weak periodic lattice potential within linear-response theory. By employing the Matsubara Green's function formalism within the low-electron-density regime, we analytically derived the static cross-susceptibility. Our results demonstrate that a purely nonmagnetic scalar potential can induce a spatially periodic real-space spin distribution. This spatial profile represents an induced spin structure rather than the emergent magnetic ordering arising from spontaneous symmetry breaking. Furthermore, symmetry analyses indicate that the spin-charge cross-response provides a direction-sensitive probe, offering a direct signature of the hidden d-wave spin-splitting.

The proportionality between χ and $Q_{k_x^2}$, i.e., in Eq. (16), holds only in the low-density continuum limit. On the other hand, χ connects

the scalar potential V to the real-space spin density $S_z(r)$, and the momentum-space spin quadrupole $Q_{k_x^2}$ shares the same $C_4\mathcal{T}$ symmetry. Hence, we expect that a qualitative positive correlation $\chi = f(Q_{k_x^2})$ remains robust beyond the low-density approximation. Certainly, the relation could become nonlinear due to band-structure effects.

The d-wave α-phase of UM and the altermagnetic state share the same symmetry pattern under rotation. If a lattice potential is imposed on the former and the latter is metallic, they cannot be distinguished by symmetry and therefore belong to the same phase according to the Landau theory of phase transitions. These arguments are based on the symmetry principle and remain valid beyond the linear-response approximation used in this manuscript.

While our continuum model with an empty-lattice approximation captures the universal symmetry properties, extending this analysis to tight-binding models exhibiting d-wave UM is highly desirable. Such an extension, particularly by incorporating multiorbital degrees of freedom, would bridge the gap between our phenomenological framework and realistic systems. Crucially, it would enable direct comparisons with emerging experimental observations, where the intricate interplay between UM orders and anisotropic Fermi surface reconstructions plays an important role.

Acknowledgments

We are grateful to Zhuang Qian for stimulating discussions. C.W. was supported by the National Natural Science Foundation of China (Grant Nos. 12234016 and 12174317). Z.P. was supported by the National Natural Science Foundation of China (Grant No. 12504219) and the startup funding from Xiamen University. This work has been supported by the New Cornerstone Science Foundation.

References

[1] Wu C and Zhang S C 2004 *Phys. Rev. Lett.* **93** 036403
[2] Wu C, Sun K, Fradkin E, and Zhang S C 2007 *Phys. Rev. B* **75** 115103
[3] Wu C 2007 online talk at Kavli Institute for Theoretical Physics, University of California, Santa Barbara
[4] Lee W C and Wu C 2009 *Phys. Rev. B* **80** 104438
[5] Oganesyan V, Kivelson S A, and Fradkin E 2001 *Phys. Rev. B* **64** 195109
[6] Jungwirth T, Fernandes R M, Fradkin E, MacDonald A H, Sinova J, and Šmejkal L 2025 *Newton* **1** 100162
[7] Šmejkal L, Sinova J, and Jungwirth T 2022 *Phys. Rev. X* **12** 040501
[8] Šmejkal L, Sinova J, and Jungwirth T 2022 *Phys. Rev. X* **12** 031042
[9] Mazin I and The PRX Editors 2022 *Phys. Rev. X* **12** 040002
[10] Liu P, Li J, Han J, Wan X, and Liu Q 2022 *Phys. Rev. X* **12** 021016
[11] Xiao Z, Zhao J, Li Y, Shindou R, and Song Z D 2024 *Phys. Rev. X* **14** 031037
[12] Chen X, Ren J, Zhu Y, Yu Y, Zhang A, Liu P, Li J, Liu Y, Li C, and Liu Q 2024 *Phys. Rev. X* **14** 031038
[13] Jiang Y, Song Z, Zhu T, Fang Z, Weng H, Liu Z X, Yang J, and Fang C 2024 *Phys. Rev. X* **14** 031039
[14] Cheong S W and Huang F T 2025 *npj Quantum Mater.* **10** 38
[15] Hayami S, Yanagi Y, and Kusunose H 2019 *J. Phys. Soc. Jpn.* **88** 123702
[16] Hayami S, Yanagi Y, and Kusunose H 2020 *Phys. Rev. B* **101** 220403
[17] Hayami S, Yanagi Y, and Kusunose H 2020 *Phys. Rev. B* **102** 144441
[18] Reimers S, Odenbreit L, Šmejkal L *et al*. 2024 *Nat. Commun.* **15** 2116
[19] Lin Z, Chen D, Lu W *et al*. 2024 arXiv:2402.04995 [cond-mat.mtrl-sci]
[20] Osumi T, Souma S, Aoyama T, Yamauchi K, Honma A, Nakayama K, Takahashi T, Ohgushi K, and Sato T 2024 *Phys. Rev. B* **109** 115102
[21] Ding J, Jiang Z, Chen X *et al*. 2024 *Phys. Rev. Lett.* **133** 206401
[22] Yang G, Li Z, Yang S *et al*. 2025 *Nat. Commun.* **16** 1442
[23] Zhang X, Liu J, Huang W, Zhang F, Zhu M Y, Zhu Y P, Chen C, Liu C, Kim C, and Shen D 2026 *Chin. Phys. Lett.* **43** 050709
[24] Song C, Bai H, Zhou Z, Han L, Reichlova H, Dil J H, Liu J, Chen X, and Pan F 2025 *Nat. Rev. Mater.* **10** 473
[25] Duan X, Zhang J, Zhu Z, Liu Y, Zhang Z, Žutić I, and Zhou T 2025 *Phys. Rev. Lett.* **134** 106801
[26] Wang Z M, Zhang Y, Zhang S B, Sun J H, Dagotto E, Xu D H, and Hu L H 2025 *Phys. Rev. Lett.* **135** 176705
[27] Zhou Z, Cheng X, Hu M, Chu R, Bai H, Han L, Liu J, Pan F, and Song C 2025 *Nature* **638** 645
[28] Jaeschke-Ubiergo R, Bharadwaj V K, Campos W, Zarzuela R, Biniskos N, Fernandes R M, Jungwirth T, Sinova J, and Šmejkal L 2025 arXiv: 2503.10797 [cond-mat.mtrl-sci]
[29] Bhattarai R, Minch P, and Rhone T D 2025 *Phys. Rev. Mater.* **9** 064403
[30] Bai H, Zhang Y, Zhou Y *et al*. 2023 *Phys. Rev. Lett.* **130** 216701
[31] Bai L, Feng W, Liu S, Šmejkal L, Mokrousov Y, and Yao Y 2024 *Adv. Funct. Mater.* **34** 2409327
[32] Chen H, Liu L, Zhou X, Meng Z, Wang X, Duan Z, Zhao G, Yan H, Qin P, and Liu Z 2024 *Adv. Mater.* **36** 2310379
[33] Jungwirth T, Sinova J, Wadley P, Kriegner D, Reichlova H, Krizek F, Ohno H, and Smejkal L 2025 arXiv:2508.09748 [cond-mat.mtrl-sci]
[34] Guo Z, Wang X, Wang W, Zhang G, Zhou X, and Cheng Z 2025 *Adv. Mater.* **37** 2505779
[35] Tian J, Li J, Liu H, Li Y, Liu Z, Li L, Li J, Liu G, and Shi J 2025 *Phys. Rev. B* **111** 035437
[36] Chen W, Zeng L, and Zhu W 2025 *Chin. Phys. Lett.* **42** 017201
[37] Feng Z, Zhou X, Šmejkal L *et al*. 2022 *Nat. Electron.* **5** 735
[38] Tschirner T, Keßler P, Gonzalez Betancourt R D *et al*. 2023 *Apl Materials* **11** 101103
[39] Sato T, Haddad S, Fulga I C, Assaad F F, and van den Brink J 2024 *Phys. Rev. Lett.* **133** 086503
[40] Attias L, Levchenko A, and Khodas M 2024 *Phys. Rev. B* **110** 094425
[41] Reichlova H, Lopes Seeger R, González-Hernández R *et al*. 2024 *Nat. Commun.* **15** 4961
[42] Leiviskä M, Rial J, Bad'ura A *et al*. 2024 *Phys. Rev. B* **109** 224430
[43] Sheoran S and Dev P 2025 *Phys. Rev. B* **111** 184407
[44] Osin A, Levchenko A, and Khodas M 2025 arXiv:2511.03151 [cond-mat.mes-hall]
[45] Liu Z, Gao Y, and Niu Q 2026 arXiv:2603.19737 [cond-mat.mes-hall]
[46] Wan W, Zhang X, Luo Y, Guo Y, and Li S 2026 arXiv:2604.03183 [cond-mat.mtrl-sci]
[47] Li D, Wang S, Li Z *et al*. 2026 arXiv:2601.01564 [cond-mat.mes-hall]
[48] Sattigeri R M, Cuono G, and Autieri C 2023 *Nanoscale* **15** 16998
[49] Ma H Y and Jia J F 2024 *Phys. Rev. B* **110** 064426
[50] Li Y X, Liu Y, and Liu C C 2024 *Phys. Rev. B* **109** L201109
[51] Li Y X 2024 *Phys. Rev. B* **109** 224502
[52] Fernandes R M, De Carvalho V S, Birol T, and Pereira R G 2024 *Phys. Rev. B* **109** 024404
[53] Parshukov K, Wiedmann R, and Schnyder A P 2025 *Phys. Rev. B* **111** 224406
[54] Li C, Hu M, Li Z *et al*. 2025 *Commun. Phys.* **8** 311
[55] Gonzalez-Hernandez R and Uribe B 2025 arXiv:2507.23173 [cond-mat.mes-hall]
[56] Du J, Peng X, Wang Y *et al*. 2025 arXiv:2509.21303 [cond-mat.mtrl-sci]
[57] Fu D, Yang L, Shen Y, Xiao K, Wang Y, Jiang W, Wang Z, Yao Y, Xue Q K, and Li W 2025 arXiv:2512.24114 [cond-mat.mtrl-sci]

Appendix A: Detailed Derivation

In this appendix, we provide the detailed derivation of the static spin-charge cross-susceptibility $\chi(\boldsymbol{G}_1)$ using the Matsubara formalism. We start from the continuum low-energy effective Hamiltonian for the d-wave α phase, subjected to a weak periodic lattice potential. In real space, the unperturbed Hamiltonian and the scalar crystal potential are respectively given by:

$$H_0 = -\frac{1}{2m}[\nabla^2 + Q(\partial_x^2 - \partial_y^2)\sigma_z] - \mu,$$

$$V(x,y) = V_0(\cos Gx + \cos Gy),$$

where $\mu = k_f^2/2m$ is the chemical potential characterized by the effective Fermi momentum k_f, and Q is the dimensionless d-wave order

parameter. Upon Fourier transforming to momentum space, the unperturbed Hamiltonian becomes block-diagonal in the spin basis:

$$H_0(\boldsymbol{k}) = \frac{1}{2m}[\boldsymbol{k}^2 + Q(k_x^2 - k_y^2)\sigma_z - k_\mathrm{f}^2],$$

where the Pauli matrix σ_z has eigenvalues $\sigma = \pm 1$ for spin-up and spin-down electrons. The periodic potential transfers momentum precisely by the primitive reciprocal lattice vectors $\boldsymbol{G}_1 = (G, 0)$ and $\boldsymbol{G}_2 = (0, G)$:

$$V(\boldsymbol{q}) = \frac{V_0}{2} \sum_{\boldsymbol{G}\in\{\pm\boldsymbol{G}_1, \pm\boldsymbol{G}_2\}} \delta_{\boldsymbol{q},\boldsymbol{G}}.$$

The noninteracting Matsubara Green's function for the system is a diagonal 2×2 matrix in spin space, $G_0(\boldsymbol{k}, \mathrm{i}\omega_n) = [\mathrm{i}\omega_n - H_0]^{-1}$, which can be written as:

$$G_0(\boldsymbol{k}, \mathrm{i}\omega_n) = \frac{1}{2}\left(\frac{1+\sigma_z}{\mathrm{i}\omega_n - \xi_\uparrow(\boldsymbol{k})} + \frac{1-\sigma_z}{\mathrm{i}\omega_n - \xi_\downarrow(\boldsymbol{k})}\right),$$

where the spin-split energy dispersions are:

$$\xi_\uparrow(\boldsymbol{k}) = \frac{1}{2m}\left(\frac{k_x^2}{a^2} + \frac{k_y^2}{b^2} - k_\mathrm{f}^2\right),$$
$$\xi_\downarrow(\boldsymbol{k}) = \frac{1}{2m}\left(\frac{k_x^2}{b^2} + \frac{k_y^2}{a^2} - k_\mathrm{f}^2\right).$$

Here, $a^{-2} = 1 + Q$ and $b^{-2} = 1 - Q$ are dimensionless scaling parameters describing the elliptical spin-dependent Fermi surfaces; equivalently, $Q = (a^{-2} - b^{-2})/2$.

To evaluate the induced spin response, we calculate the static cross-susceptibility bubble $\chi(\boldsymbol{G}_1)$ shown in Fig. 3,

$$\chi(\boldsymbol{G}_1) = T\sum_{\mathrm{i}\omega_n} \int \frac{\mathrm{d}^2\boldsymbol{k}}{(2\pi)^2} \mathrm{tr}[G(\boldsymbol{k}, \mathrm{i}\omega_n) G(\boldsymbol{k}+\boldsymbol{G}_1, \mathrm{i}\omega_n)\sigma_z].$$

Taking the trace over the spin degrees of freedom and performing the Matsubara summation, we obtain

$$\chi(\boldsymbol{G}_1) = \int_{\mathrm{BZ}} \frac{\mathrm{d}^2\boldsymbol{k}}{(2\pi)^2} \sum_\sigma \sigma \frac{n_\mathrm{F}[\xi_\sigma(\boldsymbol{k})] - n_\mathrm{F}[\xi_\sigma(\boldsymbol{k}+\boldsymbol{G}_1)]}{\xi_\sigma(\boldsymbol{k}) - \xi_\sigma(\boldsymbol{k}+\boldsymbol{G}_1)}.$$

This final form provides the analytical basis for evaluating the spin-charge cross-response at any temperature.

At zero temperature, the Fermi-Dirac distribution reduces to a step function, $n_\mathrm{F}(\xi_{\sigma k}) = \Theta(-\xi_{\sigma k})$. In the relevant metallic regime with low electron density, the occupied momenta satisfy $|\boldsymbol{k}| \ll G/2$. The occupied pockets therefore remain well separated from the zone-boundary degeneracies. The integration avoids the singularities at the Brillouin zone boundaries. By multiplying the numerator and denominator by appropriate factors, we can decompose the cross-susceptibility into four constituent integrals representing the particle and hole contributions from both spins:

$$\chi(\boldsymbol{G}_1) = 2m(-a^2 I_1 + a^2 I_2 + b^2 I_3 - b^2 I_4), \tag{A1}$$

where the integrals are explicitly given by

$$I_1(a,b) = \int_{\mathrm{BZ}} \frac{\mathrm{d}^2\boldsymbol{k}}{(2\pi)^2} \frac{\Theta[-\xi_\uparrow(\boldsymbol{k})]}{2\boldsymbol{k}\cdot\boldsymbol{G}_1 + \boldsymbol{G}_1^2},$$
$$I_2(a,b) = \int_{\mathrm{BZ}} \frac{\mathrm{d}^2\boldsymbol{k}}{(2\pi)^2} \frac{\Theta[-\xi_\uparrow(\boldsymbol{k}+\boldsymbol{G}_1)]}{2\boldsymbol{k}\cdot\boldsymbol{G}_1 + \boldsymbol{G}_1^2},$$
$$I_3(a,b) = \int_{\mathrm{BZ}} \frac{\mathrm{d}^2\boldsymbol{k}}{(2\pi)^2} \frac{\Theta[-\xi_\downarrow(\boldsymbol{k})]}{2\boldsymbol{k}\cdot\boldsymbol{G}_1 + \boldsymbol{G}_1^2}, \tag{A2}$$
$$I_4(a,b) = \int_{\mathrm{BZ}} \frac{\mathrm{d}^2\boldsymbol{k}}{(2\pi)^2} \frac{\Theta[-\xi_\downarrow(\boldsymbol{k}+\boldsymbol{G}_1)]}{2\boldsymbol{k}\cdot\boldsymbol{G}_1 + \boldsymbol{G}_1^2}.$$

with $a^{-2} = 1 + Q$ and $b^{-2} = 1 - Q$.

To calculate the unshifted integral I_1, we introduce the scale transformation $k_x = aq\cos\theta$ and $k_y = bq\sin\theta$, such that the energy dispersion becomes isotropic in the scaled coordinates: $\xi_\uparrow = (1/2m)(q^2 - k_\mathrm{f}^2)$. The integration measure is $\mathrm{d}^2\boldsymbol{k} = abq\mathrm{d}q\mathrm{d}\theta$. This yields:

$$\begin{aligned} I_1(a,b) &= \frac{ab}{2\pi}\int_0^{k_\mathrm{f}} q\mathrm{d}q \int_0^{2\pi} \frac{\mathrm{d}\theta}{2\pi} \frac{1}{2aq\cos\theta G + G^2} \\ &= \frac{ab}{2\pi}\int_0^{k_\mathrm{f}} \frac{q}{G\sqrt{G^2 - 4a^2q^2}}\mathrm{d}q \\ &= \frac{b}{8\pi a}\left[1 - \sqrt{1 - a^2\left(\frac{k_\mathrm{f}}{G/2}\right)^2}\right], \end{aligned}$$

for the shifted integral I_2, which represents the hole contribution, the parameterization shifts the origin: $k_x = aq\cos\theta - G$ and $k_y = bq\sin\theta$. Evaluating the angular integral introduces a negative sign due to the geometry of the shifted denominator, rigorously yielding $I_2(a,b) = -I_1(a,b)$.

By symmetry, the spin-down integrals are obtained simply by exchanging the parameters, $I_3(a,b) = I_1(b,a)$ and $I_4(a,b) = -I_1(b,a)$. Summing these contributions provides an analytical expression for the cross-susceptibility provided that the occupied elliptical pockets do not reach the zone boundary:

$$\begin{aligned} \chi(\boldsymbol{G}_1) &= 2m(-a^2 I_1 + a^2 I_2 + b^2 I_3 - b^2 I_4) \\ &= \frac{mab}{2\pi}\left\{\sqrt{1 - a^2\left(\frac{k_\mathrm{f}}{G/2}\right)^2} - \sqrt{1 - b^2\left(\frac{k_\mathrm{f}}{G/2}\right)^2}\right\}. \end{aligned}$$

To elucidate the role of the d-wave order, we express a and b in terms of the order parameter Q. Using $a^{-2} = 1 + Q$ and $b^{-2} = 1 - Q$, the result can be rewritten and expanded for weak d-wave UM order:

$$\chi(\boldsymbol{G}_1) = \frac{m}{2\pi}\frac{(2k_\mathrm{f}/G)^2}{\sqrt{1 - (2k_\mathrm{f}/G)^2}} Q + O(Q^2).$$

To leading order in Q, the spin response is proportional to the d-wave order parameter.

In the low-density limit $k_\mathrm{f} \ll G/2$, an expansion with respect to (k_f/G) gives the leading-order behavior:

$$\chi(\boldsymbol{G}_1) \approx -\frac{m}{4\pi}\left(\frac{k_\mathrm{f}}{G/2}\right)^2 ab(a^2 - b^2).$$

The intrinsic momentum-space spin quadrupole moment of the altermagnetic Fermi sea is defined as:

$$Q_{k_x^2} \equiv \int_{\mathrm{BZ}} \frac{\mathrm{d}^2\boldsymbol{k}}{(2\pi)^2} k_x^2 \{n_\mathrm{F}[\xi_\uparrow(\boldsymbol{k})] - n_\mathrm{F}[\xi_\downarrow(\boldsymbol{k})]\}.$$

By performing the integration over the respective elliptical areas, we obtain

$$Q_{k_x^2} = \frac{k_\mathrm{f}^4}{16\pi} ab(a^2 - b^2).$$

Thus, the induced cross-susceptibility is directly proportional to the spin quadrupole moment of the unperturbed state:

$$\chi(\boldsymbol{G}_1) = -\frac{16m}{G^2 k_\mathrm{f}^2} Q_{k_x^2}.$$

Finally, as shown in the main text, the symmetry of the spectrum $\xi_\sigma(R\boldsymbol{k}) = \xi_{-\sigma}(\boldsymbol{k})$ under a $\pi/2$ rotation guarantees that $\chi(R\boldsymbol{G}_1) = -\chi(\boldsymbol{G}_1)$. Utilizing $\boldsymbol{G}_2 = R\boldsymbol{G}_1$, the first-order correction to the real-space spin density is given as:

$$S_z(\boldsymbol{r}) = \sum_{\boldsymbol{q}\in\{\pm\boldsymbol{G}_1, \pm\boldsymbol{G}_2\}} \chi(\boldsymbol{q})\frac{V_0}{2}\exp(\mathrm{i}\boldsymbol{q}\cdot\boldsymbol{r}) = \chi(\boldsymbol{G}_1)V_0\left(\cos Gx - \cos Gy\right).$$

This links the microscopic d-wave geometry of the Fermi surface to the macroscopic spatial modulation.